www.sciencemag.org/content/354/6319/1587/suppl/DC1

Supplementary Materials for

Active cortical dendrites modulate perception

Naoya Takahashi, Thomas Oertner, Peter Hegemann, Matthew E. Larkum*

*Corresponding author. Email: matthew.larkum@hu-berlin.de

Published 23 December 2016, *Science* **354**, 1587 (2016)
DOI: 10.1126/science.aah6066

This PDF file includes:

Materials and Methods

All experiments were conducted in accordance with the guideline given by Landesamt für Gesundheit und Soziales Berlin and were approved by this authority.

Mice and head-post surgery. We used adult (>P40) C57BL/6 wild-type mice, Rbp4-Cre (#031125-UCD, MMRRC), and Sst-Cre transgenic mice (#013044, The Jackson laboratory). Mice were anaesthetized with isoflurane (1.5–2% in O_2) and kept on a thermal blanket. After the scalp and periosteum were removed, a thin layer of light-curing adhesives was applied to the skull. A light-weight head-post was fixed on the skull in the right hemisphere with a dental cement.

Chronic imaging window. A 3-mm craniotomy was made on the C2 barrel column in the left hemisphere of six wild-type and two Rbp4-Cre mice, which was functionally identified by intrinsic signal optical imaging. We found no significant difference in the proportion of discriminatory dendrites in these two populations (P = 0.22, student t-test) and therefore we pooled the data for analysis. For imaging from naïve (untrained) mice, we also used Rbp4-Cre mice. The dura was left intact. An injection micropipette (tip diameter, 5–10 μm) was filled with AAV2/1-Syn-GCaMP6s-WPRE virus solution (Penn Vector Core). The virus solution (~50 nl) was slowly injected at a depth of ~700 μm in the C2 barrel column. For experiments with Rbp4-Cre mice expressing Cre-recombinase in L5 cortical neurons, we injected 200 nl of AAV2/1-Syn-Flex-GCaMP6s-WPRE (Penn Vector Core). After injection, the craniotomy was sealed with a 3-mm glass coverslip with cyanoacrylate glue and dental cement. In some experiments, instead of the normal coverslip, we used a coverslip with a drilled access hole (~800 μm) later plugged by silicone (*34*). This allowed insertion of recording or injection pipettes under the chronic window through the access port. Imaging experiment began 4 weeks after the virus injection.

Behavior. Mice were kept on a reversed light/dark cycle. Habituation of the mice to head restraint began >5 days after the head-post or chronic window surgery. Head-restrained time at the first day was 5 min and then gradually increased each day until the mice sat calmly for 1 h. Mice were water restricted during subsequent periods of behavioral training. Weight and health of the mice were monitored daily.

Behavioral control, i.e., detecting lick events, whisker stimulation, delivering water reward, and triggering external recording devices, was performed by a custom written program running on a microcontroller board. For initial 3 or 4 training sessions, the mice received automatic water rewards (~5 µl for each trial) paired to whisker stimulation with the strongest deflection amplitude (~8º, ~1000º/s) to build an association between whisker deflection and reward. Licking was monitored using a piezo-based sensor attached to the water spout. C2 whisker was deflected by displacing a light metal bar (~3 mg) attached to the whisker using a magnetic coil placed underneath the animal. Local magnetic force was generated by loading the coil with a Gaussian-shaped current pulse (σ = 3.4 ms) via a high power amplifier. The stimulus strengths used were calibrated across the physiological range by measuring the angles of whisker deflection to different voltages applied via the amplifier to the coil. Once the mice establish the association, we introduced no-lick period and response time window in the behavioral task. After a random inter-trial interval (10–12 s for optogentic experiments with iChloC, 6–8 s for other experiments), a trial started without a preceding cue. Lick events in the 1.5 s (no-lick period) preceding the scheduled stimulus paused the trial for 6–8 s (time-out). If the mice licked the reward spout within a response window (from 0 ms to 500 or 700 ms after the stimulus onset), a drop of water was delivered through the spout. Behavioral sessions were held once or twice a day for each animal. After the mice learned the task within 1–2 weeks, we tested psychometric functions of the mice by deflecting their C2 whiskers at 7 different amplitudes including no stimulus for catch trials. Whisker stimuli with different intensities were randomly interspersed in trials. Typically, the mice needed a couple of sessions before they showed stable psychometric functions.

Two-photon Ca^{2+} imaging. Imaging from behaving animals was performed with a resonant-scanning two-photon microscope equipped with GaAsP photomultiplier tubes. GCaMP6s was excited at 940 nm (typically 20–30 mW at the sample) with a Ti:Sapphire laser and imaged through a 16×, 0.8 NA water immersion objective. Full-frame images (256 × 256 pixels) were acquired from apical dendrites of L5 neurons expressing GCaMP6s at depths of 200–300 µm at 58.6 Hz using ScanImage 4.1 software.

Electrophysiology *in vivo*. Juxtacellular recordings were performed from L5 neurons in C2 barrel column of behaving mice. Recording glass pipettes (4–7 MΩ) were filled with standard extracellular saline containing 135 mM NaCl, 5.4 mM KCl, 1.0 mM $MgCl_2$, 1.8 mM $CaCl_2$ and 5 mM HEPES (pH 7.2). The pipettes were advanced though a small craniotomy (diameter, ~0.5 mm) or the access port on the chronic glass window. Signals were amplified with Multiclamp 700B and digitized at 20 kHz by an analog-digital converter. Acquisition was performed using a custom-written Igor Pro software. To detect spikes, the signals were filtered between 300 Hz and 4 kHz. Bursts were identified as at least two spikes with an inter-spike interval of ≤ 12.5 ms (80 Hz). In Fig. 3G, non-burst-firing neurons, in which the fractions of spikes participating in burst events were less than 3%, were discarded from the analysis.

High-speed videography. Whiskers were illuminated with collimated infrared light using a high-power LED source. Images were acquired at 1000 frames/s through a 50 mm-fixed focal length lens by a high-speed CMOS camera. Image acquisition was controlled by Streampix 5.

Pharmacology. An injection micropipette was filled with 100 µM baclofen in standard extracellular saline. The pipette was inserted into the C2 barrel column through the access port on the chronic window and placed at a depth of ~200 µm beneath the pial surface. The drug was delivered by gentle pressure injection. Injections (100 nl each) were made every 20 min throughout the behavioral session. Sessions with no injections or saline injections followed the same time course as during baclofen injections. The test session was performed once per day.

Optogenetics. To directly inactivate superficial dendrites of L5 neurons, AAV2/1 (or AAV2/9)-CaMKII-iChloC-2A-tdimer2 (Viral Vector Facility of the University Medical Center Hamburg-Eppendorf) was injected at 3 sites within the C2 barrel column of four wild-type mice (~50 nl per site; depth, ~700 µm). We also conducted the same experiments with four Rbp4-Cre mice to which we made a single injection of 300 nl AAV2/9-Ef1a-DIO-iChloC-2A-DsRed vector (Viral Vector Facility of the University Medical Center Hamburg-Eppendorf). Glass window was implanted over the injection site. Optogenetic experiments were performed on the transfected mice >4 weeks after the

virus injection. iChloC-expressing dendrites were photostimulated using a 470-nm blue LED. The LED light was delivered to the C2 column using a multi-mode optic fiber (400 μm in diameter, 0.39 NA) placed 2 mm above the chronic window. The total power at the end of the fiber was 1.3–2.4 mW. Photostimulation comprised a continuous 800-ms pulse starting at –100 ms to the whisker stimulus onset, and randomly delivered on 50% of all trials. For simultaneous two-photon imaging and optogenetics, PMTs were protected by a shutter during a blue light illumination (100 ms).

For optogenetic activation of SOM cells, AAV2/1-EF1α-DIO-hChR2(H134R)-eYFP-WPRE (Penn Vector Core) was injected into the C2 barrel column of Sst-Cre mice. Injections of 100 nl were made at 350 μm and 700 μm depths below the pial surface. Photostimulation light (470 nm, 1.2–2.4 mW, 200-ms pulse starting at the whisker stimulus onset) was delivered to the C2 column via the optic fiber placed above the chronic window in 50% of all trials.

For optogenetic activation of apical dendrites of L5 neurons, AAV2/1-EF1α-DIO-hChR2(H134R)-eYFP-WPRE was injected into the C2 barrel column of Rbp4-Cre mice. An injection of 100 nl was made at a depth of 700 μm below the pial surface. A fiber-optic cannula with a mirror tip at 45˚ (200 μm in diameter, 0.37 NA) was chronically implanted to a depth of 200 μm below the cortical surface adjacent to the C2 barrel column. Photostimulation light (470 nm, 0.02–0.1 mW, 800-ms pulse starting at –100 ms to the whisker stimulus onset) was locally directed to the superficial layer of the C2 column via the implanted fiber-optic cannula.

To prevent the mice from distinguishing photostimulation trials from control trials using visual cues, the optic fiber and the chronic windows were enclosed in a black rubber cap to prevent light leakage from photostimulation into the animals' eyes. In addition to this, a masking light was continuously delivered onto the eyes via a 470 nm LED.

Measurement of light transmission in cortex. To replicate the condition of *in vivo* optogenetics with iChloC, a cortical block (3 × 3 × 3 mm) was placed upside-down on a glass coverslip and illuminated by 470-nm light via a 400-μm optic fiber positioned 2 mm underneath the coverslip. Transmitted light through different thicknesses of the

cortical tissue was measured using another 400-μm optic fiber connected to an optical power meter.

Electrophysiology *ex vivo*. Wild-type mice (>P40) were anaesthetized with isoflurane before decapitation. The brain was then rapidly transferred to ice-cold, oxygenated artificial cerebrospinal fluid (ACSF) containing 125 mM NaCl, 25 mM $NaHCO_3$, 2.5 mM KCl, 1.25 mM NaH_2PO_4, 1 mM $MgCl_2$, 25 mM glucose and 2 mM $CaCl_2$ (pH 7.4). Parasagittal slices of the primary somatosensory cortex (300-mm thick) were cut with a vibrating microslicer on a block angled at 35º to the horizontal and maintained at 37 ºC in ACSF for 30 min before use. Somatic whole-cell recordings were obtained from L5 neurons in barrel cortex. Pipettes were filled with an intracellular solution containing 135 mM K-gluconate, 7–10 mM KCl, 10 mM HEPES, 10 mM Na_2-phosphocreatine, 4 mM Mg-ATP, 0.3 mM GTP, 10mM Alexa 594 and 0.2% biocytin (pH 7.2). No correction was made for the junction potential between the bath and pipette solutions. 100 μM Baclofen in ACSF was locally applied to apical dendrites of recorded neurons through a glass pipette.

For recording from L5 neurons expressing iChloC, AAV2/1 (or AAV2/9)-CaMKII-iChloC-2A-tdimer2 was injected into the barrel cortex of P14–21 wild-type mice. An injection of 150 nl was made at a depth of 700 μm below the pial surface. Experiments were performed on the transfected mice >3 weeks after the virus injection. iChloC was locally activated by depth-calibrated 470-nm light via an optic fiber (200 μm in diameter, 0.37 NA) placed next to the soma or apical dendrite of the recorded neurons.

Histology. Animals were perfused transcardially with phosphate-buffered saline (PBS) followed by 4% paraformaldehyde (PFA). Brains were removed and post-fixed for > 24 h. After placed in 30% sucrose for > 48 h, the brains were then embedded in Optimal Cutting Temperature compound and stored at –80ºC. Coronal sections (50 μm thick) were collected using a cryostat and incubated with DAPI in PBS for 20–30 min. The sections were imaged with an epifluorescence microscope or a confocal microscope.

Data analysis. All analysis was performed using imageJ and custom written codes in Matlab.

Horizontal and vertical drifts of imaging frames due to animal motion were corrected by registering each frame to a reference image based on whole-frame cross-correlation. The reference image was generated by averaging any given consecutive 10 frames in which motion drifts were minimal. Regions of interest (ROIs) for apical dendrites of L5 neurons were manually selected with the help of average intensity and standard deviation projections across movie frames. For each ROI, pixel values inside the ROI were averaged to obtain the time series of Ca^{2+} fluorescence. Fluorescence change ($\Delta F/F_0$) was calculated as $(F - F_0)/F_0$, where F_0 was the baseline fluorescence value in the ROI throughout the whole imaging session. For the analysis in Fig. 2, we subtracted a baseline comprising the mean $\Delta F/F_0$ of the 58 frames (= 1 s) preceding the stimulus.

Psychometric parameters, i.e., detection threshold and gain (slope), were estimated by fitting detection performance across stimulus intensities with a logistic function (*35*):

$$P(x;\ \alpha, \beta, \lambda, \gamma) = \gamma + \frac{1 - \gamma - \lambda}{1 + e^{-\beta(x-\alpha)}}$$

where x is stimulus intensity, $P(x)$ is the detection probability, i.e., the fraction of 'hit' or 'false-alarm (FA)' trials, and α, β, γ, λ are free parameters that were fitted using a maximum likelihood method. Parameter α and β measure the threshold intensity and slope of the psychometric function.

To achieve comparability with psychometric functions, dendritic Ca^{2+} activity or somatic firing was quantified as neurometric functions using receiver operating characteristic (ROC) analysis (*16, 36*). Mean dendritic Ca^{2+} changes ($\Delta F/F_0$) or spike counts of L5 neurons within the 1 s following the stimulus in stimulus-present trials were compared with activities in stimulus-absent ('catch') trials. For each stimulus intensity, ROC curve was generated by plotting, for all criterion response levels, the fraction of stimulus-present trials in which the response exceeded criterion against the fraction of stimulus-absent trials in which the response exceeded criterion. The criterion level was shifted from the minimal to the maximal response observed across both trial types. Neurometric value was then computed by $(AUC - 0.5) \times 2$, where AUC is the area under the ROC curve. The value varies between –1 and 1, with 0 indicating a complete overlap between the distributions of response in stimulus-present trials and in stimulus-absent trials. The values of > 0 or < 0 indicate larger or smaller response in stimulus-

present trials than in stimulus-absent trials, respectively. Correlation between the psychometric and neurometric fucntion was quantified based on the Euclidean distance (*16*). Similarity index (SI) measures the correlation and is defined as:

$$SI = -\frac{\sqrt{\sum_i (PF_i - NF_i)^2} - \sqrt{\sum_i (PF_i)^2}}{\sqrt{\sum_i (PF_i)^2}}$$

where PF_i or NF_i denotes a value in the psychometric or neurometric function at the i-th stimulus intensity, respectively. The SIs of > 0 or < 0 indicate that the neurometric functions correlate or anti-correlate to the psychometric functions, respectively.

ROC analysis was also performed to quantify an ability of an imaged dendrite or a recorded neuron to predict the behavioral outcome at near-threshold stimuli, i.e., 'hit' or 'miss' (Fig. 2C) (*17*). Mean dendritic Ca^{2+} changes ($\Delta F/F_0$) or spike counts of L5 neurons within the 1 s following the stimulus in hit trials were compared with activities in miss trials. We analyzed the trials with two stimulus intensities around the animal's detection threshold. The ROC curve was then obtained by the same procedure as described above. Discrimination index (DI) was defined as $DI = (AUC - 0.5) \times 2$. DI ranges from –1 to 1, where the value of < 0 means ''negative responses in hit trials'', > 0 means ''positive responses in hit trials,'' and 0 represents "no difference in responses between hit and miss trials. Statistical significance of DI was assessed by a permutation test, for which the sampling distribution was obtained from 10,000 resampled datasets by exchanging labels ('hit' or 'miss') on trials.

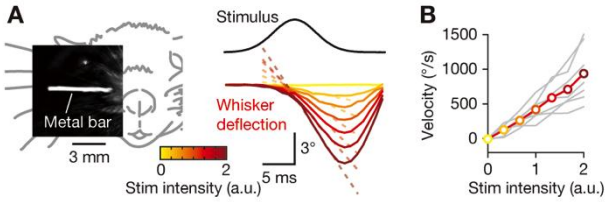

Fig. S1. Magnetic deflection of targeted single whisker

(**A**) (Left) High-speed (1000 frames/s) videography of whisker deflection. A small metal bar was attached to the C2 whisker of an anesthetized mouse and deflected by a magnetic coil (*10*). (Right) Average deflection angles of the whisker stimulated at various intensities (n = 7 mice). (**B**) Angular velocity linearly increases as a function of stimulus intensity. Mean amplitude and velocity (color) obtained from 7 mice plotted with individual data (gray).

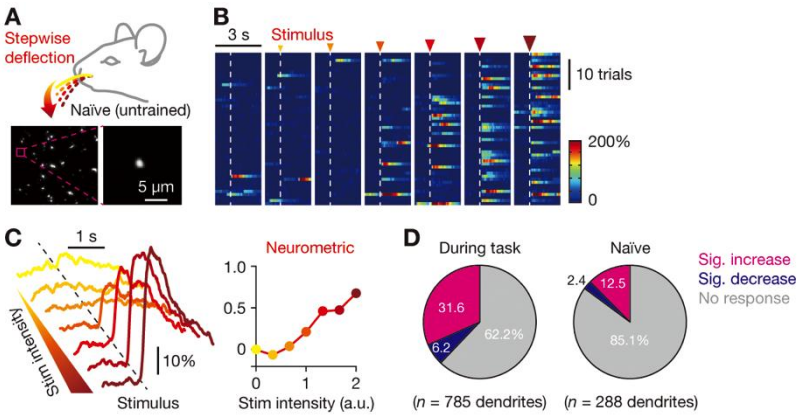

Fig. S2. Apical dendritic Ca^{2+} response to whisker stimulation in naïve mice

(**A**) Two-photon Ca^{2+} imaging from the apical dendrites of L5 neurons in the C2 barrel column of naïve (untrained) mice. (**B**) Ca^{2+} signals in the apical dendrite marked in (A) organized according to increasing stimulus intensity (columns). (**C**) Averaged Ca^{2+} responses to various stimulus intensities (left) and neruometric function (right) of the dendrite in (A) and (B). (**D**) Fraction of apical dendrites with significant neurometric values (i.e., increase or decrease in dendritic Ca^{2+} activity) at salient (maximum) stimuli in trained mice during the detection task (n = 785 dendrites from 8 mice, left) and in naïve mice (n = 288 dendrites from 3 mice, right). The significance of neurometric values was determined by a permutation test ($P < 0.05$).

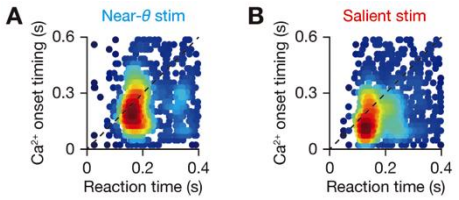

Fig. S3. Timing of apical dendritic Ca^{2+} relative to licking response

(**A**) Onset timing of the near-threshold stimulus-evoked Ca^{2+} events in dendrites with *DI > 0 plotted against the timing of animal's first (rewarded) licks (reaction time) (*n* = 1,136 events). Color indicates data density (hot colors are higher density). (**B**) Same as (A) for salient stimulus (*n* = 1,022 events).

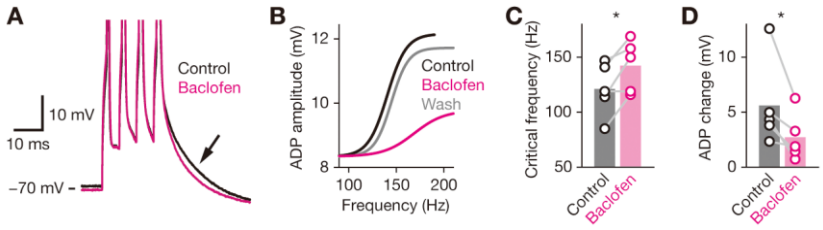

Fig. S4. Baclofen blocks Ca^{2+} spike generation in L5 pyramidal neurons

(**A**) Patch-clamp recording *ex vivo* from L5 pyramidal neuron, while baclofen (50 µM) was puff-applied onto apical dendrites. Baclofen blocked ADP increase (arrow) – a measure of dendritic Ca^{2+} spike (*28*) – evoked by high-frequency trains of APs. (**B**) Fitted curves for ADP amplitudes as a function of AP train frequency. (**C**) Effect of baclofen on critical frequency (n = 5 cells, $*P$ = 0.035). (**D**) Effect of baclofen on ADP amplitude change (n = 5 cells, $*P$ = 0.044). Statistical significance was determined by paired t-test.

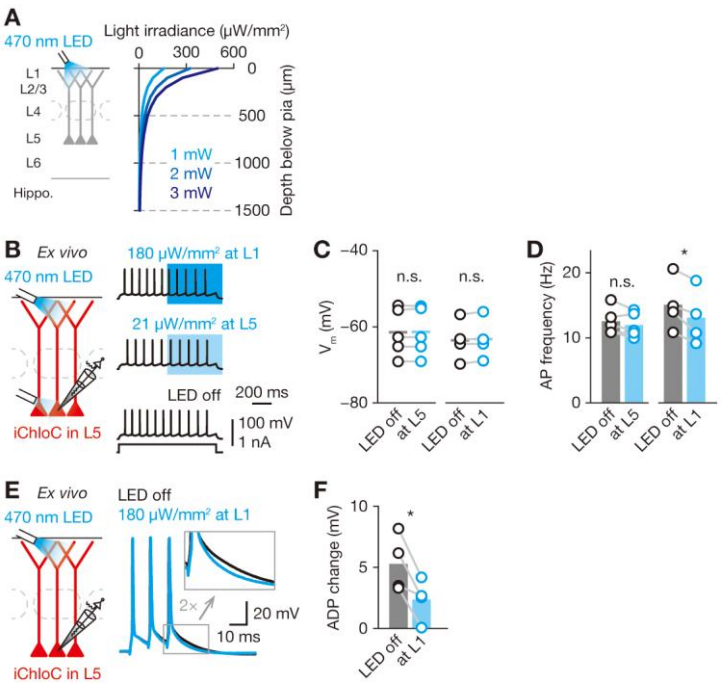

Fig. S5. Depth-calibrated iChloC activation suppresses dendritic Ca^{2+} spike, but not somatic action potential generation

(**A**) (Left) Direct measurement of 470-nm light transmission in mouse cortical tissue. (Right) Averaged light irradiance (blue) at different cortical depths (*n* = 2 cortical blocks). Three different intensities of LED light were tested: 1, 2 and 3 mW, spanning the range of intensities used *in vivo* with iChloC (1.3 to 2.4 mW; avg. 1.90 ± 0.35 mW). (**B**) (Left) Patch-clamp recording in brain slices *ex vivo* from L5 pyramidal neuron expressing iChloC, while recreating the *in vivo* depth-calibrated light intensity profile estimated in (A). (Right) Somatic AP response to suprathreshold current injection (300 pA) in the presence of depth-calibrated 470-nm light at L5 or L1 (700 μm or 100 μm below the pia, respectively). (**C**) Somatic membrane potential (V_m) without (LED off) and with iChloC activation at L5 or L1 (*n* = 5 cells, *P* = 0.63 for LED at L5; *n* = 4 cells, *P* = 0.23 for LED at L1). (**D**) Frequency of evoked APs with and without iChloC activation at L5 or L1 (*n* = 5 cells, *P* = 0.18 for LED at L5; *n* = 4 cells, **P* = 0.019 for LED at L1). (**E**) iChloC activation at L1 blocked Ca^{2+} spikes in apical dendrites as seen in a decrease in ADP size at soma (c.f., effect of baclofen in fig. S3). (**F**) Effect of iChloC activation at L1 on ADP amplitude change (*n* = 4 cells, **P* = 0.026). Statistical significance was determined by paired *t*-test.

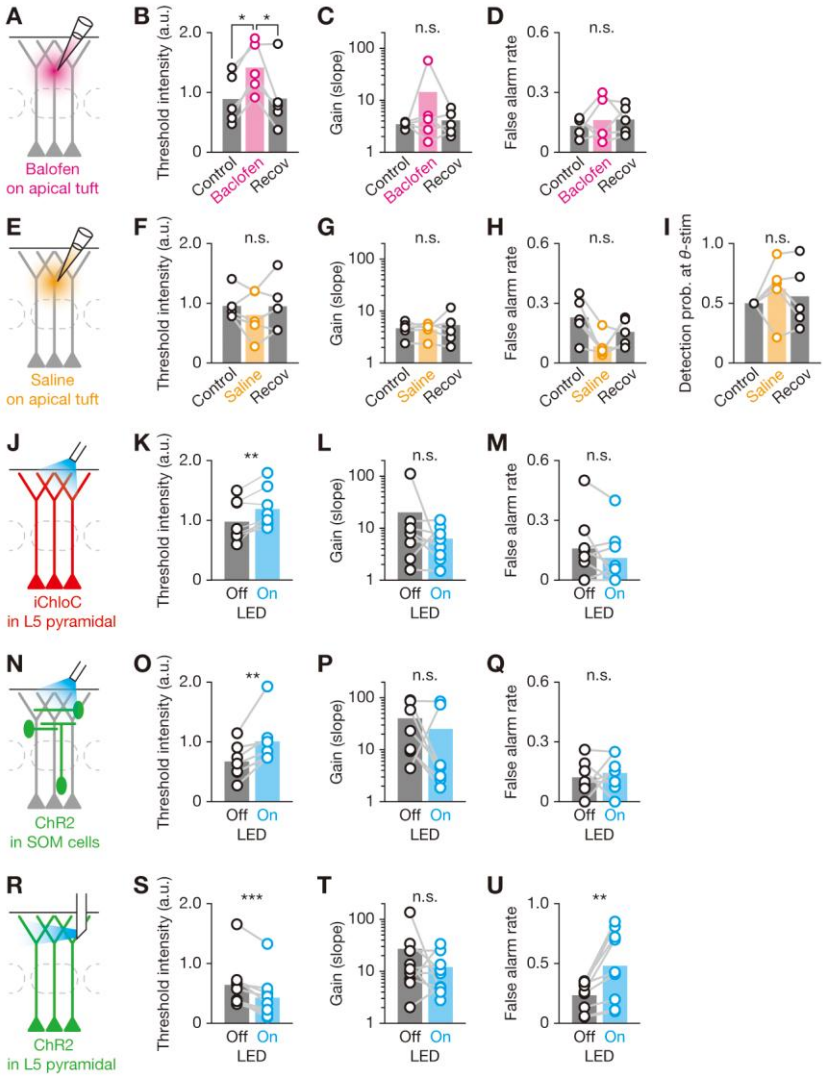

Fig. S6 Psychometric parameter changes during manipulation of dendritic activity

(**A** to **D**) Psychometric parameters while apical dendrites of L5 neurons were treated with baclofen (n = 5 mice). (**B**) Threshold intensity (*P < 0.05). (**C**) Gain (P = 0.42). (**D**) False alarm rate (P = 0.76). (**E** to **I**) Local application of extracellular saline (n = 5 mice). (**F**) Threshold intensity (P = 0.34). (**G**) Gain (P = 0.70). (**H**) Detection probability at the threshold stimulus intensity (P = 0.52). (**I**) False alarm rate (P = 0.065). (**J** to **M**) Dendritic inactivation via activating iChloC in superficial dendrites of L5 neurons (n = 8 mice). (**K**) Threshold intensity (**$P = 6.4 \times 10^{-3}$). (**L**) Gain (P = 0.34). (**M**) False alarm rate (P = 0.23). (**N** to **Q**) Dendritic inactivation via activating SOM cells expressing ChR2 (n = 7 mice). (**O**) Threshold intensity (**$P = 8.0 \times 10^{-3}$). (**P**) Gain (P = 0.44). (**Q**)

False alarm rate (P = 0.93). (**R** to **U**) Dendritic activation via activating ChR2 in superficial dendrites of L5 neurons (n = 9 mice). (**S**) Threshold intensity (***$P = 2.6 \times 10^{-4}$). (**T**) Gain (P = 0.35). (**U**) False alarm rate (**$P = 5.9 \times 10^{-3}$). Statistical significance in (A to I) and in (J to U) was determined by paired t-test with Bonferroni's correction after one-way repeated-measures ANOVA and paired t-test, respectively.

References

1. M. Murayama, M. E. Larkum, Enhanced dendritic activity in awake rats. *Proc. Natl. Acad. Sci. U.S.A.* **106**, 20482–20486 (2009). doi:10.1073/pnas.0910379106 Medline

2. N. L. Xu, M. T. Harnett, S. R. Williams, D. Huber, D. H. O'Connor, K. Svoboda, J. C. Magee, Nonlinear dendritic integration of sensory and motor input during an active sensing task. *Nature* **492**, 247–251 (2012). doi:10.1038/nature11601 Medline

3. F. Gambino, S. Pagès, V. Kehayas, D. Baptista, R. Tatti, A. Carleton, A. Holtmaat, Sensory-evoked LTP driven by dendritic plateau potentials in vivo. *Nature* **515**, 116–119 (2014). doi:10.1038/nature13664 Medline

4. J. Cichon, W. B. Gan, Branch-specific dendritic Ca^{2+} spikes cause persistent synaptic plasticity. *Nature* **520**, 180–185 (2015). doi:10.1038/nature14251 Medline

5. M. E. Larkum, J. J. Zhu, B. Sakmann, A new cellular mechanism for coupling inputs arriving at different cortical layers. *Nature* **398**, 338–341 (1999). doi:10.1038/18686 Medline

6. M. Larkum, A cellular mechanism for cortical associations: An organizing principle for the cerebral cortex. *Trends Neurosci.* **36**, 141–151 (2013). doi:10.1016/j.tins.2012.11.006 Medline

7. W. A. Phillips, A. Clark, S. M. Silverstein, On the functions, mechanisms, and malfunctions of intracortical contextual modulation. *Neurosci. Biobehav. Rev.* **52**, 1–20 (2015). doi:10.1016/j.neubiorev.2015.02.010 Medline

8. D. J. Felleman, D. C. Van Essen, Distributed hierarchical processing in the primate cerebral cortex. *Cereb. Cortex* **1**, 1–47 (1991). doi:10.1093/cercor/1.1.1 Medline

9. K. S. Rockland, in *Extrastriate Cortex in Primates*, K. S. Rockland, J. H. Kaas, A. Peters, Eds. (Plenum Press, New York, 1997), pp. 243–293.

10. S. Sachidhanandam, V. Sreenivasan, A. Kyriakatos, Y. Kremer, C. C. Petersen, Membrane potential correlates of sensory perception in mouse barrel cortex. *Nat. Neurosci.* **16**, 1671–1677 (2013). doi:10.1038/nn.3532 Medline

11. S. Manita, T. Suzuki, C. Homma, T. Matsumoto, M. Odagawa, K. Yamada, K. Ota, C. Matsubara, A. Inutsuka, M. Sato, M. Ohkura, A. Yamanaka, Y. Yanagawa, J. Nakai, Y. Hayashi, M. E. Larkum, M. Murayama, A top-down cortical circuit for accurate sensory perception. *Neuron* **86**, 1304–1316 (2015). doi:10.1016/j.neuron.2015.05.006 Medline

12. S. E. Kwon, H. Yang, G. Minamisawa, D. H. O'Connor, Sensory and decision-related activity propagate in a cortical feedback loop during touch perception. *Nat. Neurosci.* **19**, 1243–1249 (2016). doi:10.1038/nn.4356 Medline

13. B. Libet, W. W. Alberts, E. W. Wright Jr., B. Feinstein, Responses of human somatosensory cortex to stimuli below threshold for conscious sensation. *Science* **158**, 1597–1600 (1967). doi:10.1126/science.158.3808.1597 Medline

14. J. F. Corso, A theoretico-historical review of the threshold concept. *Psychol. Bull.* **60**, 356–370 (1963). doi:10.1037/h0040633 Medline

15. R. P. Rao, D. H. Ballard, Predictive coding in the visual cortex: A functional interpretation of some extra-classical receptive-field effects. *Nat. Neurosci.* **2**, 79–87 (1999). doi:10.1038/4580 Medline

16. M. C. Stüttgen, C. Schwarz, Psychophysical and neurometric detection performance under stimulus uncertainty. *Nat. Neurosci.* **11**, 1091–1099 (2008). doi:10.1038/nn.2162 Medline

17. D. H. O'Connor, S. P. Peron, D. Huber, K. Svoboda, Neural activity in barrel cortex underlying vibrissa-based object localization in mice. *Neuron* **67**, 1048–1061 (2010). doi:10.1016/j.neuron.2010.08.026 Medline

18. L. M. Palmer, J. M. Schulz, S. C. Murphy, D. Ledergerber, M. Murayama, M. E. Larkum, The cellular basis of $GABA_B$-mediated interhemispheric inhibition. *Science* **335**, 989–993 (2012). doi:10.1126/science.1217276 Medline

19. G. Doron, M. von Heimendahl, P. Schlattmann, A. R. Houweling, M. Brecht, Spiking irregularity and frequency modulate the behavioral report of single-neuron stimulation. *Neuron* **81**, 653–663 (2014). doi:10.1016/j.neuron.2013.11.032 Medline

20. E. Pérez-Garci, M. E. Larkum, T. Nevian, Inhibition of dendritic Ca^{2+} spikes by $GABA_B$ receptors in cortical pyramidal neurons is mediated by a direct $G_{i/o}$-βγ-subunit interaction with Ca_v1 channels. *J. Physiol.* **591**, 1599–1612 (2013). doi:10.1113/jphysiol.2012.245464 Medline

21. J. Wietek, R. Beltramo, M. Scanziani, P. Hegemann, T. G. Oertner, J. Simon Wiegert, An improved chloride-conducting channelrhodopsin for light-induced inhibition of neuronal activity in vivo. *Sci. Rep.* **5**, 14807 (2015). doi:10.1038/srep14807 Medline

22. G. Silberberg, H. Markram, Disynaptic inhibition between neocortical pyramidal cells mediated by Martinotti cells. *Neuron* **53**, 735–746 (2007). doi:10.1016/j.neuron.2007.02.012 Medline

23. M. Murayama, E. Pérez-Garci, T. Nevian, T. Bock, W. Senn, M. E. Larkum, Dendritic encoding of sensory stimuli controlled by deep cortical interneurons. *Nature* **457**, 1137–1141 (2009). doi:10.1038/nature07663 Medline

24. L. J. Gentet, Y. Kremer, H. Taniguchi, Z. J. Huang, J. F. Staiger, C. C. H. Petersen, Unique functional properties of somatostatin-expressing GABAergic neurons in mouse barrel cortex. *Nat. Neurosci.* **15**, 607–612 (2012). doi:10.1038/nn.3051 Medline

25. M. Carandini, A. K. Churchland, Probing perceptual decisions in rodents. *Nat. Neurosci.* **16**, 824–831 (2013). doi:10.1038/nn.3410 Medline

26. F. Helmchen, K. Svoboda, W. Denk, D. W. Tank, In vivo dendritic calcium dynamics in deep-layer cortical pyramidal neurons. *Nat. Neurosci.* **2**, 989–996 (1999). doi:10.1038/14788 Medline

27. M. Murayama, E. Pérez-Garci, H. R. Lüscher, M. E. Larkum, Fiberoptic system for recording dendritic calcium signals in layer 5 neocortical pyramidal cells in freely moving rats. *J. Neurophysiol.* **98**, 1791–1805 (2007). doi:10.1152/jn.00082.2007 Medline

28. M. E. Larkum, K. M. Kaiser, B. Sakmann, Calcium electrogenesis in distal apical dendrites of layer 5 pyramidal cells at a critical frequency of back-propagating action potentials.

Proc. Natl. Acad. Sci. U.S.A. **96**, 14600–14604 (1999). doi:10.1073/pnas.96.25.14600 Medline

29. T. Bachmann, How a (sub)cellular coincidence detection mechanism featuring layer-5 pyramidal cells may help produce various visual phenomena. *Front. Psychol.* **6**, 1947 (2015). Medline

30. K. Meyer, The role of dendritic signaling in the anesthetic suppression of consciousness. *Anesthesiology* **122**, 1415–1431 (2015). doi:10.1097/ALN.0000000000000673 Medline

31. S. Palva, K. Linkenkaer-Hansen, R. Näätänen, J. M. Palva, Early neural correlates of conscious somatosensory perception. *J. Neurosci.* **25**, 5248–5258 (2005). doi:10.1523/JNEUROSCI.0141-05.2005 Medline

32. B. Pleger, A. Villringer, The human somatosensory system: From perception to decision making. *Prog. Neurobiol.* **103**, 76–97 (2013). doi:10.1016/j.pneurobio.2012.10.002 Medline

33. S. C. Murphy, L. M. Palmer, T. Nyffeler, R. M. Müri, M. E. Larkum, Transcranial magnetic stimulation (TMS) inhibits cortical dendrites. *eLife* **5**, e13598 (2016). doi:10.7554/eLife.13598 Medline

34. C. J. Roome, B. Kuhn, Chronic cranial window with access port for repeated cellular manipulations, drug application, and electrophysiology. *Front. Cell. Neurosci.* **8**, 379 (2014). doi:10.3389/fncel.2014.00379 Medline

35. R. D. Wimmer, L. I. Schmitt, T. J. Davidson, M. Nakajima, K. Deisseroth, M. M. Halassa, Thalamic control of sensory selection in divided attention. *Nature* **526**, 705–709 (2015). doi:10.1038/nature15398 Medline

36. K. H. Britten, M. N. Shadlen, W. T. Newsome, J. A. Movshon, The analysis of visual motion: A comparison of neuronal and psychophysical performance. *J. Neurosci.* **12**, 4745–4765 (1992). Medline